High-resolution resonance Bragg-scattering spectroscopy of an atomic transition from a population difference grating in a vapour cell

2010 J. Phys. B: At. Mol. Opt. Phys. 43 135403

(http://iopscience.iop.org/0953-4075/43/13/135403)

J. Phys. B: At. Mol. Opt. Phys. **43** (2010) 135403 (5pp) doi:10.1088/0953-4075/43/13/135403

High-resolution resonance Bragg-scattering spectroscopy of an atomic transition from a population difference grating in a vapour cell

Hai Wang[1], **Xudong Yang, Ling Zhang, Shujing Li, Chunhong Zhang, Changde Xie and Kunchi Peng**

The State Key Laboratory of Quantum Optics and Quantum Optics Devices, Institute of Opto-Electronics, Shanxi University, Taiyuan 030006, People's Republic of China

E-mail: wanghai@sxu.edu.cn.

Received 3 December 2009, in final form 25 April 2010
Published 14 June 2010
Online at stacks.iop.org/JPhysB/43/135403

Abstract

We present a novel high-resolution backward resonance Bragg-scattering (RBS) spectroscopy from a population difference grating (PDG). The PDG in thermal ^{87}Rb vapour is formed by a standing-wave (SW) pump field, which periodically modulates the space population distributions of two levels in the ^{87}Rb D1 line. A probe beam, having identical frequency and orthogonal polarization with the SW pump field, is Bragg-scattered by the PDG. The Bragg-scattered light is strongest at an atomic transition, and forms an RBS spectrum with a high signal-to-noise and sub-natural linewidth (60% of the natural linewidth). The observed RBS is a type of degenerate four-wave-mixing signal and can also be explained with the coherent superposition of the optical fields Rayleigh-scattered from the oscillating dipole moments of individual atoms on the PDG.

(Some figures in this article are in colour only in the electronic version)

The techniques of Doppler-free laser spectroscopy [1] such as saturated absorption and two-photon laser spectroscopy invented in the early 1970s have had a marked impact on the field of precision spectroscopy. These techniques have been applied in a variety of modern scientific and technical fields, for example, stabilization of the laser frequency for cooling atoms [2], measurements of absolute optical frequency of atoms [3, 4], test of relativistic time dilation [5] and optical frequency metrology [6]. The accuracy of the optical frequency measurements of atomic transitions relies on the full width at half maximum (FWHM) and the signal-to-noise ratio (S/N) of the laser spectrum [7].

It has been well known that a strong standing-wave (SW) optical field in an atomic medium can induce various atomic gratings. The optical lattices loading cold atoms created by the interaction of the off-resonance SW field are typical atomic density gratings; Bragg scattering from such a grating has been demonstrated [8, 9]. In a three-level EIT atomic system with a stronger SW coupling field, the absorptive properties of the atomic medium is spatially modulated; thus, an electromagnetically induced grating (EIG) is formed. Bragg reflection from the EIG has been experimentally demonstrated in vapour cells [10–12]. For the past three decades, four-wave-mixing (FWM) processes [13–21] in various atomic media have been extensively studied theoretically and experimentally, and the used FWM configuration is generally the backward geometry. In this configuration two pump beams, called forward (F) and backward (B) beams, propagate through the atomic medium in the z and $-z$ directions, respectively, while a probe (P) beam is incident on atoms at a small angle θ to the z direction; thus, a FWM signal propagating in the opposite direction of the P beam is generated. Such a FWM signal was interpreted as Bragg scattering from an atomic population grating formed by the interference of the P and F beams [14, 18]. In usual

[1] Author to whom any correspondence should be addressed.

degenerate four-wave-mixing (DFWM) experiments [14–17], the DFWM spectral lines were measured by synchronously scanning the frequency of the three (*P, F* and *B*) beams, and the observed DFWM spectrum is Doppler free (the linewidth is somewhat larger than the natural linewidth). For example, in cold Cs atoms [17], the achieved DFWM spectral linewidth of the $F = 1$ to $F' = 2$ transition is ∼9 MHz, which is larger than the 5.3 MHz natural linewidth of the Cs transition. In atomic vapours, the observed DFWM spectral linewidths of D2 transitions in Cs atoms and Na atoms are ∼10 MHz [16] and ∼30 MHz [14], respectively. In the recent experiments of FWM [19–21] and Bragg reflection from EIG [12], the frequency of one beam was locked to a fixed detuning from an atomic resonance, and the frequency of other laser beams was scanned across another atomic transition to observe the FWM or Bragg reflection signal. Due to the long-lived ground-state coherence [12, 19, 20] or long-lived polarizability wave [21], the observed spectral signal was sub-natural linewidths. Although the linwidths of these FWM spectra are extremely narrow, the spectral signals are strongly affected by the fixed frequency detuning [12, 19, 20] and vary along with the detuning amount. Therefore the sub-natural spectroscopy has not been applied so far in the measurement of the atomic transition frequency.

Here, by scanning all three laser frequencies together, we demonstrate a novel high-resolution resonance Bragg-scattering (RBS) spectroscopy from an atomic population difference grating (PDG) in a thermal Rb atomic cell. The configuration of our experimental system is different from that in the previous experiments on DFWM [12–20]. In the experimental configuration, two *x*-polarized pump beams propagate through Rb atoms in the z (forward) and $-z$ (backward) directions, respectively, and a *y*-polarized probe beam is incident on the atoms in the z direction ($\theta = 0$). In this case, a population difference grating was created by the interference between the two *x*-polarized forward (*F*) and backward (*B*) pump beams in the atomic vapour and the *y*-polarized probe (*P*) beam is scattered from the PDG. The generated backward Bragg-scattering light can be separated from the direction of the *B* beam with a Glan-laser prism. Using a simple theoretical model, we give an explanation of why the linewidth of the Bragg-scattering spectroscopy (RBS) is below the natural linewidth. In the theoretical model, Bragg scattering is regarded as the result of the constructive interference of the optical fields Rayleigh-scattered from the oscillating dipole moments of the individual atoms on the PDG, which points out that there is some relationship between Bragg scattering and Rayleigh scattering. We also show that Bragg scattering is a type of DFWM. The experimentally observed narrowest linewidth is ∼3.5 MHz, which is less than the Rb natural linewidth of ∼5.8 MHz. Unlike the previous works in which sub-natural linewidths were observed [18–20], the feature observed here appears only at the atomic resonance.

The presented scheme for demonstrating RBS spectroscopy with a narrow linewidth can be understood by a simple model. As shown in figure 1, the states $|\mathrm{b}\rangle$ and $|\mathrm{a}\rangle$ are the ground and excited states of ^{87}Rb atoms, respectively, and the state $|\mathrm{c}\rangle$ is a non-radiatively coupled state. An *x*-polarized SW pump field $\boldsymbol{E}_{\mathrm{SW}}(t) = \boldsymbol{E}_F(t) + \boldsymbol{E}_B(t)$ and a *y*-polarized probe (*P*) field $\boldsymbol{E}_P(t) = \boldsymbol{e}_y \boldsymbol{E}_P\, \mathrm{e}^{-\mathrm{i}\omega t - \mathrm{i}k_P z}$ both couple to the $|\mathrm{b}\rangle$ to $|\mathrm{a}\rangle$ transition, where $\boldsymbol{E}_F(t) = \boldsymbol{e}_x \boldsymbol{E}_F\, \mathrm{e}^{-\mathrm{i}\omega t - \mathrm{i}\boldsymbol{k}_F z}$ and $\boldsymbol{E}_B(t) = \boldsymbol{e}_x E_B\, \mathrm{e}^{-\mathrm{i}\omega t - \mathrm{i}\boldsymbol{k}_B z}$ are *x*-polarized forward (*F*) and backward (*B*) propagating pump fields, respectively. $\boldsymbol{k}_F$, $\boldsymbol{k}_B$ and $\boldsymbol{k}_P$ are the wave vectors for the *F, B* and *P* beams, where $\boldsymbol{k}_F = -\boldsymbol{k}_B = \boldsymbol{k}_P = \boldsymbol{k}$. $\boldsymbol{e}_x$ and $\boldsymbol{e}_y$ are the unit vectors along the x and y axes, respectively. Under the condition of the weak probe field, the steady-state population difference $\Delta\rho(z) = \rho_{bb}(z) - \rho_{aa}(z)$ of the atoms can be expressed as [22]

$$\Delta\rho(z) \propto \frac{E_F^* E_B \cos 2kz}{(\Delta^2 + (\Gamma/2)^2)}, \tag{1}$$

where $\rho_{bb}(z)$ and $\rho_{aa}(z)$ are the populations in $|\mathrm{b}\rangle$ and $|\mathrm{a}\rangle$, respectively, Γ is the natural linewidth of ^{87}Rb atoms and $\Delta = \omega - \omega_{ba}$ is the frequency detuning. From equation (1), one can see that $\Delta\rho(z)$ is modulated along the z axis due to the optical pumping of the SW field. At the node positions of $z = (m + 1/2)\pi/k$ ($m = 0, 1, 2, \ldots$), $\Delta\rho(z)$ reaches the maximum, while at the antinode positions of $z = m\pi/k$, $\Delta\rho(z)$ has the minimum; thus, a PDG with a period $d = \pi/k = \lambda/2$ is formed. Note that the Doppler frequency shifts due to atomic motion have not been considered in the above expression, and thus equation (1) can be used just to calculate the population of the atoms with speeds of $v_z \approx 0$. Since the Doppler-free configuration is used in the presented scheme, the atoms with speeds of $v_z \approx 0$ will give large contributions to $\Delta\rho(z)$ and thus equation (1) can be considered as a good approximate expression.

When the near-resonance probe field $\boldsymbol{E}_P(t)$ interacts with the two-level atoms, it will be strongly scattered. The scattered light contains both elastic (Rayleigh) and inelastic scattered components [23]. The inelastic components are incoherent, and do not contribute to Bragg scattering. The Rayleigh components resulting from the radiation of the oscillating atomic dipole are coherent, and the constructive interference of these components forms the RBS spectrum in the present experiment. The ratio of the intensity of the coherently scattered light to the total scattering intensity has been discussed in Mollow's paper [23], in which they predicted that the scattering light should be almost completely coherent in the limit of the weak probe. The Rayleigh-scattering field ε_s from a dipole oscillator driving by the probe field is proportion to its dipole moment, i.e. $\varepsilon_s \propto \langle \ddot{\mu}(t) \rangle$. The expectation value of the oscillating dipole moment induced by the *y*-polarized probe field can be written as [22]

$$\langle \boldsymbol{\mu}_y(t, z) \rangle \propto \frac{\boldsymbol{E}_p(t, z)\Delta\rho(z)}{(\Delta + \mathrm{i}\Gamma/2)} + \mathrm{c.c}, \tag{2}$$

which is considered to be parallel to the *y*-polarized direction. The total Rayleigh-scattered field is the sum of the radiation field of each dipole oscillator within the interaction region (volume *V*). We divide the interaction volume V into many small element volumes $\delta V = A\delta z$, where $A = \pi d^2/4$ is the area of the cross section of the probe beam and d is the diameter of the beam. For a volume element δV with $d \gg \lambda$, Rayleigh scattering only appears in the forward and backward directions if the atomic medium is homogeneous in density number [22]. The backward Rayleigh-scattered (reflected) field δE_s from

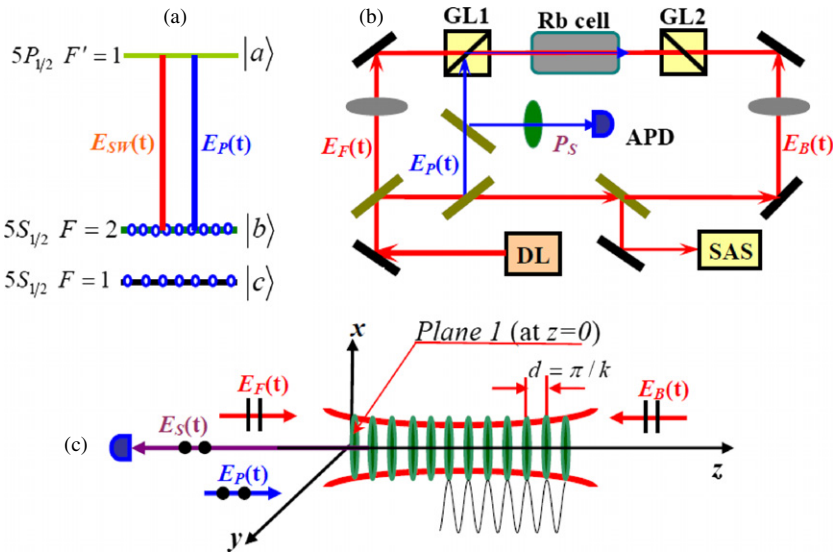

Figure 1. Essential experimental information. (a) Relevant energy levels of the ^{87}Rb atom. (b) The schematic of experimental set-up. DL is an external-cavity diode laser with a bandwidth ∼0.5 MHz during a short scanning time (∼50 ms). GL1 and GL2 are two Glan-laser prisms with an extinction ratio 10^5, APD is an avalanche detector, SAS is a rubidium saturated absorption spectrometer. (c) The schematic of the RBS spectrum from the PDG, which is formed by a SW pump field.

the atoms within the volume element δV at the z position can be written as

$$\delta \boldsymbol{E}_s \propto \frac{\ddot{P}_y(t - z/c)\delta V}{4\pi\varepsilon_0 c^2}, \tag{3}$$

where the polarization $P_y(t - z/c)$ is given by

$$\boldsymbol{P}_y(t, z) = \boldsymbol{\mu}_y(t, z)N_0. \tag{4}$$

N_0 is the number of the atoms within a very small volume element δV. Introducing equation (4) into equation (3), we can express the reflected field δE_s from the volume element δV as

$$\delta \boldsymbol{E}_s \propto \frac{E_P\, \mathrm{e}^{-\mathrm{i}2kz}}{(\Delta + \mathrm{i}\Gamma/2)}\Delta\rho(z_i)N_0 A\delta z. \tag{5}$$

Equation (5) shows that the amplitude of the reflected field δE_S from the volume element δV at the position z is proportional to the population difference $\Delta\rho(z)$, and the phase of the field δE_S from the volume element δV at the position z is $-2kz$ when it travels to the left end ($z = 0$) of the atomic medium. For the present atomic medium with a PDG, the fields δE_S from the volume element δV at the node positions are stronger than those from δV at the antinode positions. The two stronger scattered fields δE_S respectively from two adjacent nodes δV undergo constructive interference since the PDG period length d is $\lambda/2$, and thus the backward Bragg scattering is generated. The backward Bragg scattering can be viewed as the DFWM process. The generated signal field (Bragg scattering field) $E_S(t) = E_s\, \mathrm{e}^{-\mathrm{i}k_S z - \mathrm{i}\omega t}$ can be obtained by introducing the expression for the polarization (equation (5)) into the wave equation for nonlinear optical media [22]. We obtained

$$\frac{dE_s}{\mathrm{d}z} \propto \frac{\mathrm{e}^{-\mathrm{i}(k_P - k_S)z + \mathrm{i}(k_F - k_B)z}}{(\Delta + \mathrm{i}\Gamma/2)(\Delta^2 + (\Gamma/2)^2)} E_F^* E_P E_B N_0. \tag{6}$$

Equation (6) shows that the DFWM phase matching condition $\boldsymbol{k}_F - \boldsymbol{k}_B = \boldsymbol{k}_P - \boldsymbol{k}_S$ will be satisfied when the generated signal field has a wave vector $\boldsymbol{k}_s = -\boldsymbol{k}_P$.

From equation (6), we obtained the reflected signal power [22]

$$P_S \propto \frac{P_F P_B P_P l^2}{((\Gamma/2)^2 + \Delta^2)^3}, \tag{7}$$

where $P_{F(B,P)}$ is the power of the $E_F(E_B, E_P)$ field. From equation (7), we can see that P_S depends on the detuning Δ and the strongest P_S appears at the atomic resonance, which forms the RBS spectrum. The calculated FWHM linewidth of the RBS spectrum equals 0.51 Γ. The physical reason to produce such a narrow spectrum is that the RBS has a non-Lorentzian function $[\Delta^2 + (\Gamma/2)^2]^{-3}$, which is different from the Lorentzian function $[\Delta^2 + (\Gamma/2)^2]^{-1}$ with an atomic natural linewidth of Γ.

The experimental set-up for the RBS spectrum is shown in figure 1(b). A laser beam, coming from an external-cavity diode laser (Toptica DL100, with a 0.5 MHz FWHM laser linewidth), is divided into three beams by the beam splitters. One serves as the probe beam, the other two are used for the forward (F) and backward (B) pump beams. The Glan prisms GL1 and GL2 are inserted respectively in the F and B pump beams to make two optical beams be in x axis polarization. The two pump beams overlap in a Rb vapour cell to build a SW (as shown in figure 1(c)). The probe (P) beam overlaps with the F pump beam on GL1 and the output probe beam is polarized along the y direction. The signal light Bragg-scattered from the PDG propagates along the −z direction in the cell and is reflected by GL1 and the beam splitter (BS), and is finally detected by an avalanche detector. The atomic cell is $l = 5$ cm long and its temperature is stabilized at about 91 °C. Since the Zeeman-sublevel shifts induced by the background magnetic field may broaden the linewidthes of laser spectrum, we wrapped the atomic cell in μ-metal to shield the background magnetic field. The measured resident magnetic field is less than 20 mG. The radii of all probe and pump beams are about 1 mm at the centre of the cell. We

scanned the frequency of the DL (diode laser) across the transition $F = 2$ to $F' = 1$ to measure the backward RBS spectrum; the sweep rate is 15 MHz ms^{-1}. The FWHM linewidth of the RBS spectrum was calibrated with the half of the frequency splitting (408.3 MHz) between the states $5P_{1/2}$ $F' = 1$ and $F' = 2$, which is measured by the saturated absorption spectrometer.

Firstly, fixing the F pump power P_F (300 μW) and the probe power P_P (32 μW), the RBS spectra are measured under different powers of the B beam (P_B = 56, 80, 100, 130, 160, 210, 252 μW, respectively). The measured RBS spectra are shown in figures 2(a)–(g) with the blue curves, whose centres correspond to the centre of SAS spectra. From figure 2(a), we can see that the FWHM of RBS spectrum is ∼3.5 MHz at P_B = 56 μW. The red dashed curves in the insets of figures 2(a)–(d) are the theoretical fits using the function $\left[\Delta^2 + \left(\frac{\Gamma}{2}\right)^2 G^2\right]^{-3}$, the fitting parameter G depends on the light intensity of the B beam. Increasing the power P_B, the intensity of the SW pump field is enhanced and the population modulation of the atoms is also strengthened, which results in a stronger RBS signal. Simultaneously, the FWHM linewidth of RBS spectrum gradually increases to ∼6 MHz due to the influence of the saturated effect. The linewidths of all RBS spectra in figures 2(a)–(f) are narrower than the natural atomic linewidth of $\Gamma \approx 5.8$ MHz. Figure 2(h) is the measured RBS spectrum with $P_F = 440$ μW, $P_B = 300$ μW, $P_P = 32$ μW. In this case the signal intensity of the RBS spectrum is increased, while the FWHM linewidth is simultaneously broadened to ∼9 MHz. When P_P is increased to $P_P = 552$ μW and P_F and P_B are set to 440 μW and 300 μW, respectively, the signal peak power of RBS is increased to ∼3.5 μW and the linewidth is broaden to ∼13 MHz (figure 2(i)). The signal-to-noise ratio in figure 2(i) is ∼2000, which is mainly limited by the electronic noise and the measurement bandwidth of the detection system. From figures 2(a)–(i), it is pointed out that the intensity and the linewidth of the RBS spectrum depend on P_F, P_B and P_P. In experiments, we can adjust the three powers respectively to obtain the optimal RBS spectrum according to different requirements.

It is interesting that when any one of the three beams (P, F and B) is blocked, the RBS spectrum will totally disappear. The black (red) curve in figure 2(j) is the measured RBS signal in the absence of the F (B) beam, where the RBS spectroscopy signal disappears, that is, because the PDG no longer exists. The blue curve in figure 2(j) is the measured Bragg-scattered light in the absence of the P beam, of course, the RBS spectrum also does not exist because there is no incident probe field.

Figure 3(a) is the measured peak powers $P_{SP}(P_S|_{\Delta=0})$ of RBS spectra as a function of P_B, the inset shows its linewidth versus P_B. The peak powers P_{SP} go slowly up when P_B increases for P_B <160 μW, which is not in agreement with the theoretical prediction from equation (7). We consider that the RBS light may be affected by the atomic absorption; this fact is not involved in equation (7). When P_B >160 μW, the peak powers P_{SP} increase approximately proportional to P_B linearly, which is in agreement with equation (7). Figures 3(b) and (c) are the measured peak powers P_{SP} of RBS spectroscopy

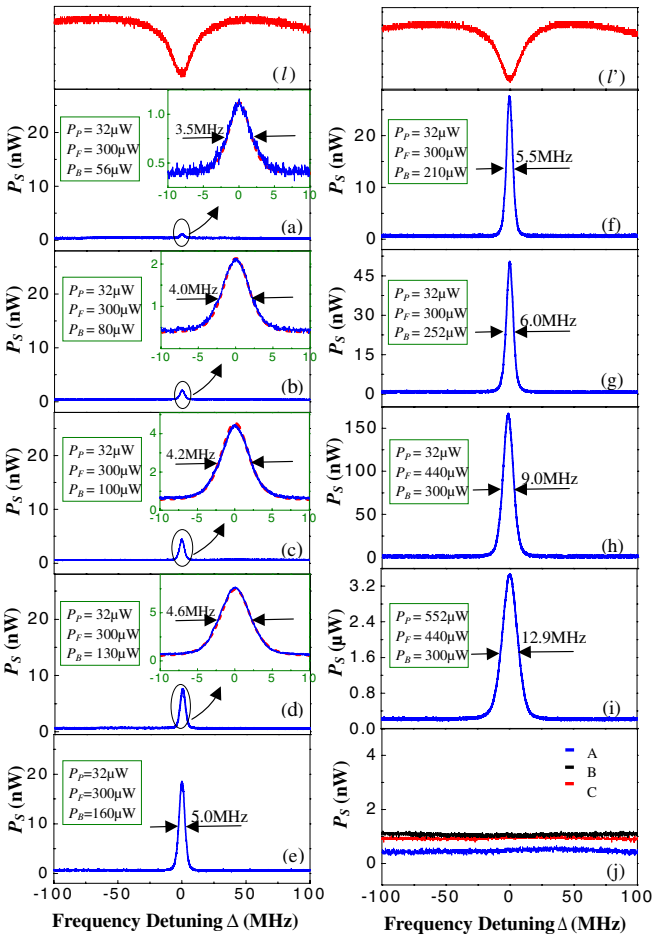

Figure 2. The measured RBS spectrum for different P_B, P_F and P_P. (a)–(g) The measured RBS spectrum at P_F = 300 μW and P_P = 32 μW for P_B =56, 80, 100, 130, 160, 210, 252 μW, respectively. The red (dotted) curves in the insets of (a)–(d) are the theoretical fits using the function $[\Delta^2 + (\Gamma/2)^2 G^2]^{-3}$, G is the fitting parameter. (h) The measured RBS spectrum for P_F = 440 μW, P_P = 32 μW and P_B = 300 μW. (i) The measured RBS spectrum for P_F = 440 μW, P_P = 552 μW and P_B = 300 μW. (j) The measured results when one of the three beams (backward and forward pump (B, F), and probe P beams) is blocked. The powers of the three beams are set at P_F = 300 μW, P_B = 100 μW, P_P = 100 μW. The red, black and blue traces correspond to the cases without B, F or P, respectively.

as the function of P_F and P_P, respectively. The insets are the corresponding linewidths. The data in figure 3(b) (figure 3(c)) show that P_{SP} linearly depends on P_F (P_P), which is in good agreement with the prediction from equation (7). We define a frequency resolution $F_M = \frac{\Delta v_{1/2}}{SNR}$ (where SNR [24] is the signal-to-noise ratio, $\Delta v_{1/2}$ is the FWHM linewidth of the RBS spectrum) to characterize the performance of the observed RBS spectrum. The data in figures 3(a′), (b′) and (c′) are the frequency resolution as the function of P_B, P_F and P_P, respectively. In figure 3(c′), the minimum frequency resolution reaches ∼0.003 and it is far less than that obtained from [3] (in which, the evaluated frequency resolution is ∼0.08).

In conclusion, we presented a high-resolution backward resonance Bragg-scattering (RBS) spectroscopy from a population difference grating (PDG). By increasing the power of P_F (P_B or P_P), it is possible to achieve an RBS spectrum

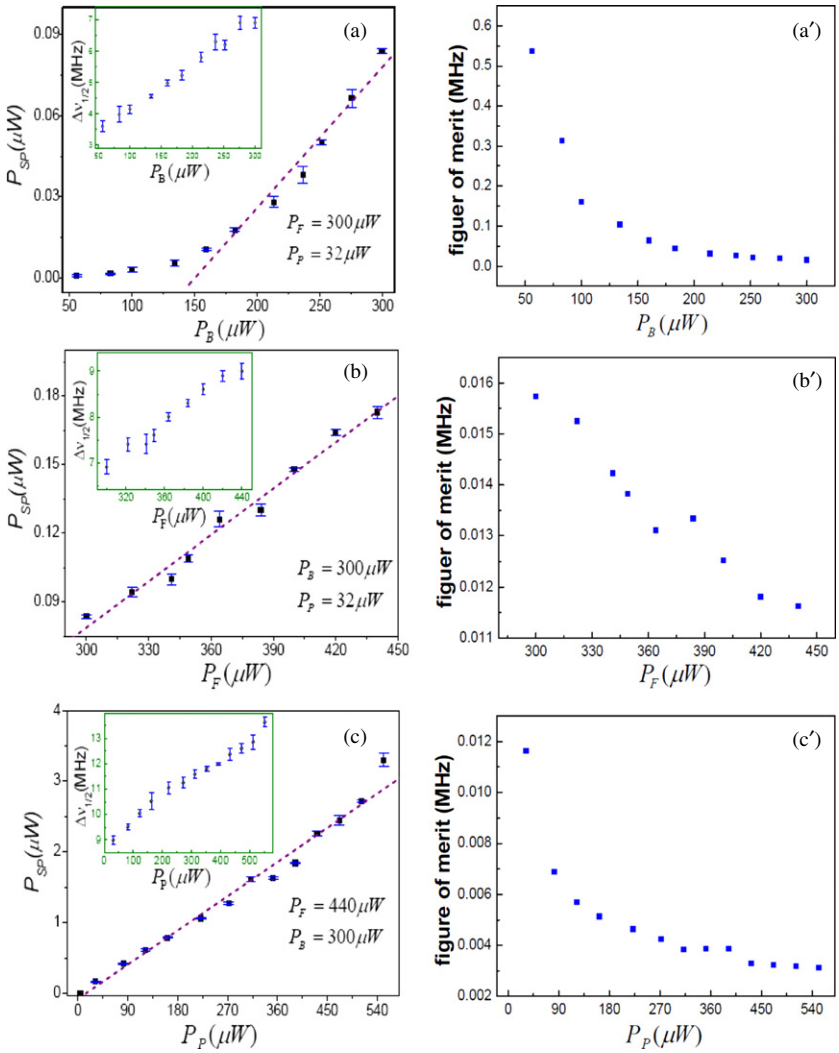

Figure 3. (a), (b) and (c) are the dependences of the peak power P_{SP} (i.e. $P_S|_{\Delta=0}$) of the RBS spectrum on P_B (a), P_F (b) and P_P (c), respectively. The insets in (a), (b) and (c) show the dependences of the linewidth of the RBS spectroscopy on P_B, P_F and P_P, respectively. (a′), (b′) and (c′) Frequency resolution as the function of P_F, P_B and P_P.

with a required S/N and narrower linewidth based on the presented system. These properties provide us with a potential to develop a high-resolution spectroscopy for accurately measuring atomic transitions. We believe that the present scheme of RBS has potential applications in precise frequency measurements.

Acknowledgment

We acknowledge funding support from the National Natural Science Foundation of China (no 10874106, 60736040, 60821004), and the 973 Program (2010CB921103).

References

[1] Hänsch T W 2006 *Rev. Mod. Phys.* **78** 1297
[2] Lindquist K, Stephens M and Wieman C 1992 *Phys. Rev.* A **46** 4082
[3] Udem T, Reichert J, Holzwarth R and Hänsch T W 1999 *Phys. Rev. Lett.* **82** 3568
[4] Gerginov V *et al* 2006 *Phys. Rev.* A **73** 032504
[5] Reinhardt S *et al* 2007 *Nat. Phys.* **3** 861
[6] Hong F-L *et al* 1999 *IEEE Trans. Instrum. Meas.* **48** 532
[7] Hall J L and Ye J 2001 *Opt. Photonics News* **12** 45
[8] Birkl G *et al* 1995 *Phys. Rev. Lett.* **75** 2823
[9] Weidemüller M *et al* 1995 *Phys. Rev. Lett.* **75** 4583
[10] Bajcsy M, Zibrov A S and Lukin M D 2003 *Nature* **426** 638
[11] Brown A W and Xiao M 2005 *Opt. Lett.* **30** 699
[12] Bae I-H *et al* 2008 *Appl. Opt.* **47** 4849
[13] Yariv A and Pepper D M 1977 *Opt. Lett.* **1** 16
[14] Liao P F, Bloom D M and Economou N P 1978 *Appl. Phys. Lett.* **32** 813
[15] Oria M, Bloch D, Fichet M and Ducloy M 1989 *Opt. Lett.* **14** 1082
[16] Ai B, Glassner D S and Knize R J 1994 *Phys. Rev.* A **50** 3345
[17] Tabosa J W R *et al* 1997 *Phys. Rev.* A **55** 2968
[18] Cardoso G C *et al* 1999 *Phys. Rev.* A **59** 1408
[19] Cardoso G C and Tabosa J W R 2002 *Phys. Rev.* A **65** 033803
[20] Barreiro S and Tabosa J W R 2005 *Phys. Rev.* A **71** 013405
[21] Hemmerich A, Weidemuller M and Hansch T 1994 *Europhys. Lett.* **27** 427
[22] Boyd R W 1992 *Nonlinear Optics* (New York: Academic)
[23] Mollow B R 1969 *Phys. Rev.* **188** 1969–75
[24] Snyder J J, Raj R K, Bloch D and Ducloy M 1980 *Opt. Lett.* **5** 163